Earth and Planetary Science Letters 603 (2023) 117982

Contents lists available at ScienceDirect

Earth and Planetary Science Letters

journal homepage: www.elsevier.com/locate/epsl

Hydrated komatiites as a source of water for TTG formation in the Archean

Tamblyn R. [a,*], Hermann J. [a], Hasterok D. [b], Sossi P. [c], Pettke T. [a], Chatterjee S. [a]

[a] Institut für Geologie, Universität Bern, Bern, Switzerland
[b] Department of Earth Sciences, University of Adelaide, Adelaide, Australia
[c] Institut für Geochemie und Petrologie, ETH Zurich, Zurich, Switzerland

ARTICLE INFO

Article history:
Received 18 August 2022
Received in revised form 19 December 2022
Accepted 27 December 2022
Available online 10 January 2023
Editor: R. Hickey-Vargas

Keywords:
TTG
komatiite
Archean
water cycle
crust formation

ABSTRACT

The preserved Archean continental crust is dominantly comprised of tonalite-trondhjemite-granodiorite (TTG) suites associated with less abundant low-grade greenstone belts. The exact processes that form TTGs, as well as the source rock they are derived from, are difficult to constrain from the sparse Archean geological record. However, studies show that the water-present partial melting of metamorphosed basalt at temperatures of 750–950 °C is required to produce large volumes of partial melt with TTG compositions. In this contribution, we investigate if hydrated komatiites — a constituent of greenstone belts — played a vital role in TTG genesis. Using petrology, mineral chemistry and phase equilibria modelling of representative komatiite samples, combined with analysis of a global geochemical dataset of komatiites and basaltic komatiites, we show that during metamorphism hydrated komatiites can release at least 6 weight % mineral-bound water. Up to 5 weight % of this water is released by breakdown of chlorite and tremolite at temperatures between 680 and 800 °C, regardless of the P–T path (i.e., tectonic scenario) experienced by the komatiitic rocks. As the temperatures of komatiite dehydration are above the water-saturated basalt solidus, the released water can trigger voluminous partial melting of basalt to ultimately create TTG batholiths. This considerable hydration potential of komatiites is due to their high X_{Mg} (X_{Mg} = molar Mg/[Mg+Fe]), which stabilises water-rich minerals during oceanic alteration on the seafloor, but also extends the stability of Mg-rich chlorite to high temperatures. During prograde metamorphism, the X_{Mg}, CaO and Al_2O_3 content of the reactive rock composition determines the proportion of chlorite vs amphibole, and therefore the volume of water which can be transported to temperatures of >750 °C. Despite the low abundance of komatiites in greenstone belts, they potentially played a vital role in crustal formation and the Earth's early water cycle.

1. Introduction

On modern Earth, continental crust is primarily generated through intermediate-felsic magmatism in arc settings (e.g. Rudnick, 1995; Taylor and McLennan, 1995; Jagoutz and Kelemen, 2015). Subducted mafic-ultramafic rocks trap and transport water (sensu lato) from the oceanic floor and release this water via dehydration reactions during subduction-related metamorphism. This water percolates into the mantle wedge triggering hydrous melting to form basalts, which either form the primary melts of arc magmatism, or which underplate the arc and cause fluid-fluxed melting of the lower crust (Grove et al., 2012; Collins et al., 2016). The role of water in this process is unarguably critical, and its availability controls arc melting processes and sets the mean andesitic-dacitic chemical composition of the continental crust, and therefore all rocks formed from it (Rudnick, 1995; Taylor and McLennan, 1995: Jagoutz and Kelemen, 2015). By contrast, the surviving Archean cratons are dominated (>80% by volume; Polat, 2012) by tonalite-trondhjemite-graniodiorite suites (TTGs; Fig. 1), suggesting that they were the major constituent of early continental crust. The general consensus is that TTGs are sourced from partial melting of hydrous metabasalt, i.e., an amphibolite (e.g. Drummond and Defant, 1990; Arculus and Ruff, 1990; Foley et al., 2002; Moyen and Martin, 2012). Variations in source basalt chemistry, melting depth and temperature, mixing of melt compositions, degree of partial melting, and subsequent fractional crystallisation all cause variations in TTG chemistry (Moyen and Stevens, 2006; Getsinger et al., 2009; Hoffmann et al., 2014).

An emergent feature of TTGs is that many were formed at intriguingly low temperatures (750–950 °C from Ti saturation tem-

* Corresponding author.
E-mail address: renee.tamblyn@geo.unibe.ch (R. Tamblyn).

https://doi.org/10.1016/j.epsl.2022.117982

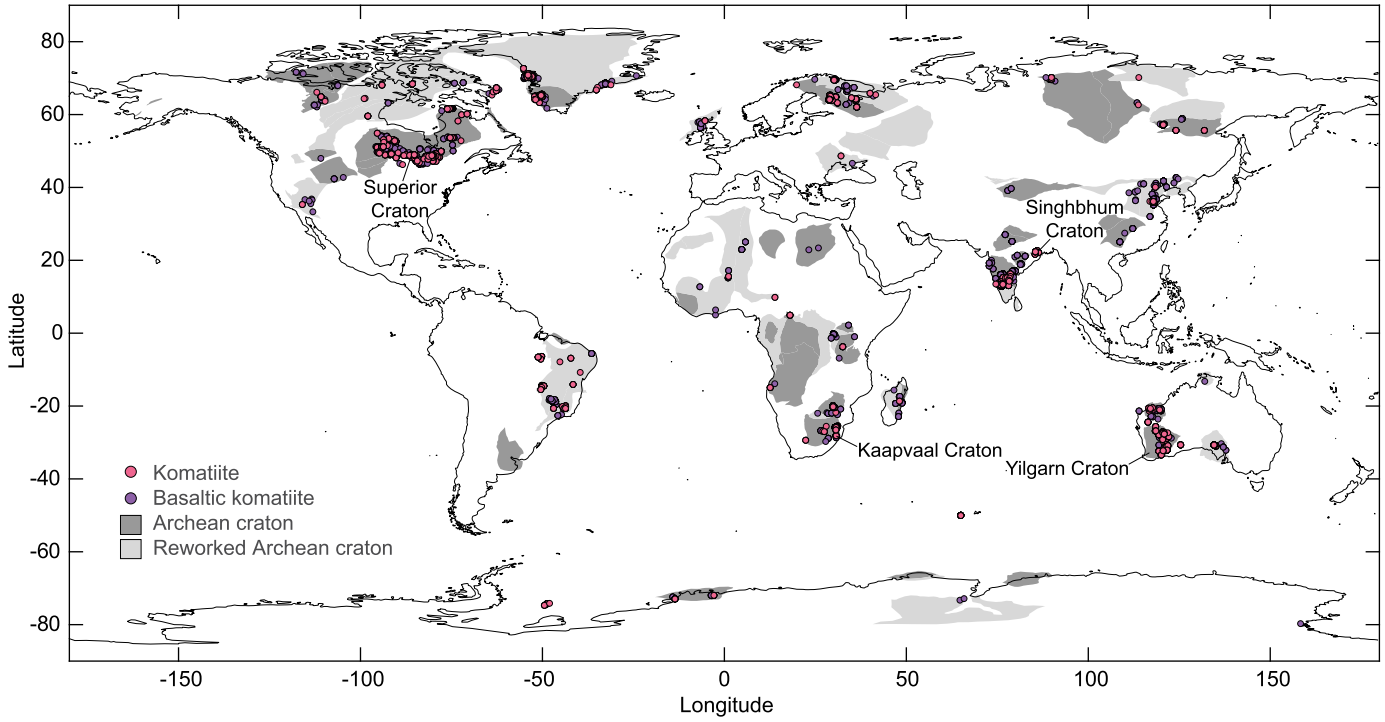

Fig. 1. Locations of komatiites and basaltic komatiites from Archean cratons or reworked Archean cratons from the updated geochemical dataset of Gard et al. (2019; Supp. Table 2). Archean cratons are defined as not having experienced significant metamorphism or reworking since the Archean, and reworked Archean cratons are generally defined as having experienced significant geological reworking after the Archean, after Hasterok et al. (2022). The locations of cratons with representative samples from this study are highlighted.

peratures; Xiong et al., 2009). These estimates are supported by experimental data (e.g., Qian and Hermann, 2013) and phase equilibria models of melts produced from rocks with basaltic compositions (e.g., Johnson et al., 2017; Pourteau et al., 2020; Kendrick and Yakymchuk, 2020). Voluminous partial melting of basaltic rocks at these low temperatures calls for contributions of free water (i.e. a water-bearing fluid; e.g., Lambert and Wyllie, 1972; Pourteau et al., 2020), as amphibole dehydration melting of basalt will only produce low melt fractions below ~950 °C (Lambert and Wyllie, 1972; Rapp and Watson, 1995). As amphibolite-facies metabasalt itself cannot provide the amount of free water needed at these conditions, various tectonic mechanisms for transport of fluid to the deep crust have been suggested to trigger wet basalt melting, including modern-style subduction (e.g., Laurie and Stevens, 2012). Nevertheless, the source of free fluid at lower crustal conditions in the Archean has remained elusive, with the suggestion that hydrated ultramafic rocks like komatiites may hold the key (Hartnady et al., 2022).

The remaining ~20% of Archean cratons are comprised of greenstone belts. These belts are commonly metamorphosed to greenschist or lower amphibolite facies conditions, and contain sequences of felsic volcanic rocks, clastic and chemical sedimentary rocks, tholeiitic basalts, basaltic komatiites and komatiites. Of particular interest are komatiites, highly magnesian (>18 wt.% MgO) extrusive rocks, with eruption temperatures of up to 1700 °C (Nisbett et al., 1993; Arndt et al., 2008; Wilson, 2019). They occur as lava flows comprising cumulate and spinifex zones with chilled margins, or less often as shallow intrusions (Nisbett et al., 1993; Arndt et al., 2008). These melts are likely sourced from mantle plumes, which sample the lower to upper mantle (Arndt, 2003; Wilson and Bolhar, 2022), although some argue that they may represent Archean oceanic crust (Furnes and Dilek, 2022) or formed in supra-subduction settings (Parman et al., 2004). Most komatiites are Archean–Paleoproterozoic in age, and are the signature of a higher ambient mantle temperature on the early Earth (Herzberg et al., 2007). All Archean komatiites are hydrated and metamorphosed, comprising serpentine, chlorite, and amphibole-bearing assemblages (Arndt, 2003; Sossi et al., 2016), as many were likely erupted onto the seafloor and hydrated through interaction with seawater, and later metamorphosed to greenschist-amphibolite facies. While this technically marks all Archean komatiitic rocks as metakomatiites, we use the term komatiites for simplicity.

Recently, it has been suggested from mineral equilibria modelling that high-MgO mafic rocks, including komatiites, from greenstone belts may have played a critical role in the capture and release of water during prograde metamorphism in the Archean, leading to the formation of TTGs (Hartnady et al., 2022). In this study we combine data from the petrology and phase equilibria modelling of a representative komatiite from the Barberton Greenstone belt, the mineral chemistry of metamorphosed komatiite samples from key greenstone belts worldwide, and a global compilation of geochemical data from 5589 komatiites and komatiitic basalts (Fig. 1). We show that komatiites can contain significant amounts of mineral-bound water in antigorite ($[Mg,Fe^{2+}]_3Si_2O_5(OH)_4$), chlorite ($[Mg,Fe^{2+}]_{10}Al_2[Al_2Si_6O_{20}](OH)_{16}$) and tremolite ($Ca_2Mg_5Si_8O_{22}(OH)_2$). During prograde metamorphism this water is released via dehydration reactions above the water-saturated basalt solidus (>650 °C), promoting low temperature fluid-present melting of basalt to generate voluminous TTGs, regardless of the style of tectonics operating in the Archean.

2. Materials

2.1. Kaapvaal craton

To investigate mineral breakdown reactions by phase equilibria modelling, a representative metamorphosed komatiite from the ca. 3.5 Ga Komati formation of the Barberton Greenstone Belt (BGB), Kaapval Craton, South Africa (Fig. 1), was selected, based on its mineralogy, bulk rock composition and mineral compositions. This

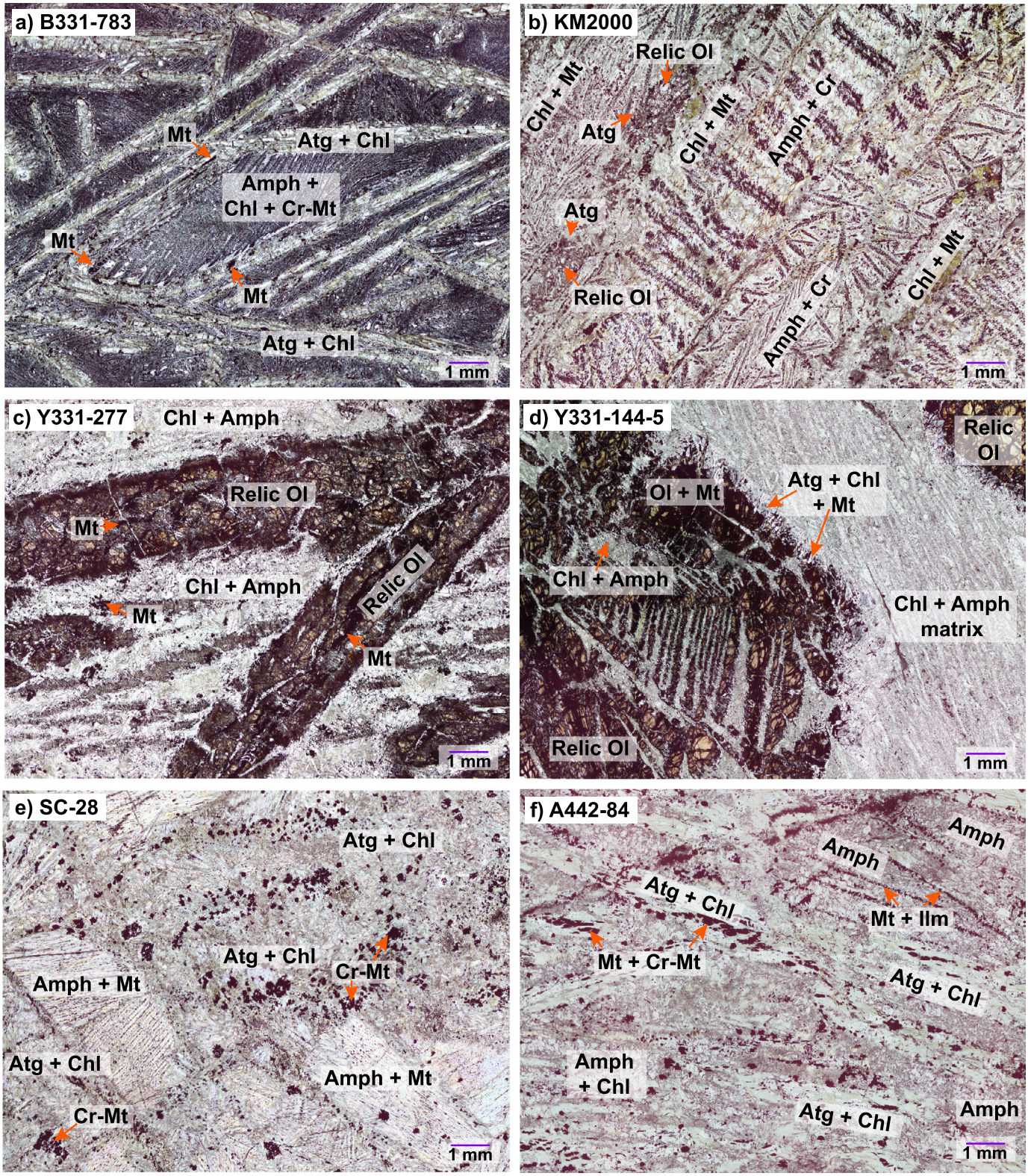

Fig. 2. Photomicrographs of representative metamorphosed komatiites, many show spinifex textures inherited from primary olivine. B331-783 and KM2000 are from the Kaapval Craton, Y331-277 and Y331-144-5 are from the Yilgarn Craton, SC28 is from the Singhbhum Craton, and A422-84 is from the Superior Craton. Atg: Antigorite, Chl: Chlorite, Amph: Amphibole, dominantly tremolitic in composition, Mt: Magnetite, Cr-Mt: Chrome-rich magnetite, Cr: Chromite, Ilm: Ilmenite, Ol: Olivine.

sample, B331-783, is an Al-depleted komatiite from Sossi et al. (2016) and Nesbitt et al. (1979). It exhibits spinifex textures, presumably once olivine, now completely pseudomorphed by antigorite, chlorite and chromian magnetite (Fig. 2a). The spinifex psuedomorphs are up to 3 cm long and randomly oriented. The matrix is now a finer-grained mass of tremolite, chlorite, magnetite and ilmenite, which are oriented in elongate fan and linear structures (Fig. 2a). Rare fine-grained titanite clusters often form on the margins of the spinifex. There are no relic igneous phases preserved in the sample. Sample KM2000 is from the Komati Formation at

Spinifex Creek, it exhibits coarse-grained (up to 5 cm) spinifex textures with relic olivine that is partially replaced by antigorite, in a tremolite and chlorite matrix (Fig. 2b). Chromite is the dominant oxide mineral, with less abundant magnetite and ilmenite.

2.2. Yilgarn craton

Two samples from Yakabindie (Y331-277) and Mt. Burges (Y331-144-5) are from the ca. 2.7 Ga Norseman-Wiluna belt in the Yilgarn Craton, Australia (Nesbitt and Sun, 1976; Fig. 1). Both are Al-undepleted and show coarse spinifex-textures with relic igneous olivine. The Yakabindie sample contains antigorite and chlorite partially pseudomorphing olivine, which forms spinifex up to 3 cm long, in a matrix of metamorphic tremolite, chlorite, magnetite, ilmenite and less than 1 volume % calcite (Fig. 2c). The Mt. Burges sample contains antigorite + magnetite and amphibole forming corona on olivine grain boundaries, and chlorite, amphibole and magnetite replacing olivine along fractures, surrounded by a matrix of tremolite, chlorite and ilmenite (Fig. 2d).

2.3. Singhbhum craton

One sample of basaltic komatiite was analysed from the ca. 3.3–3.45 Ga ultramafic unit, belonging to Eastern Iron Ore Group (EIOG) of the Singhbhum Craton, India (Fig. 1). Sample SC28 is from the Potka locality, where rocks of the lower Badampahar sequence of EIOG are exposed, and contains the mineral assemblage amphibole (mostly tremolitic), antigorite, chlorite, chromian magnetite and ilmenite (Fig. 2e).

2.4. Superior craton

One komatiite sample is from the ca. 2.7 Ga Abitibi Belt, Superior Craton, Canada (Fig. 1). It is sample A442-84 from Sossi et al. (2016). It contains oriented spinifex-textures which are up to 1 cm in length, now completely pseudomorphed by antigorite, chlorite and magnetite with chromian-magnetite rims, in a matrix of finer-grained amphibole, chlorite, magnetite and ilmenite (Fig. 2f).

3. Methods

3.1. Electron probe micro analysis

Electron Probe Micro Analysis of chlorite, antigorite, amphibole, and accessory minerals was performed using a JEOLJXA-8200 superprobe, housed at the Institute of Geological Sciences, University of Bern. Spot analyses and quantitative maps were collected. Spot analyses for chlorite, amphibole, magnetite and ilmenite used a 15 keV accelerating voltage, 20 nA current and a 40 s dwell time on peak and 20 s each on the background positions. Spot analyses for antigorite used a 5 nA beam current. Ten element oxides were calibrated using natural and synthetic standards, including albite (Na_2O), almandine (SiO_2, Al_2O_3, FeO), anorthite (CaO), forsterite (MgO), ilmenite (TiO_2), tephroite (MnO), chromium spinel (Cr_2O_3) and a pure metal oxide standard (NiO_2). These spot analyses were used as internal standards to quantify an X-ray intensity map for B331-783, resulting in quantitative compositional maps. The maps were acquired by WDS with 15 keV accelerating voltage, a 100 nA current and 100 ms dwell time on peak for each spot and 20 s on background positions, over an area of 6 x 6 mm. Ten elements were measured across two successive passes, and Na was measured on the first scan. The compositional maps were processed with XMapTools 4 to identify minerals (Lanari et al., 2014, 2019), and were used to generate the reactive rock composition (Table 1; Fig. 3a) and mineral proportions (modes; Fig. 3b).

Table 1
Calculated rock compositions in molar % for sample B331-783, the compositions from this study (H_2O only and $XCO_2 = 1$) were used for phase equilibria modelling, the measured bulk rock is also presented for comparison. Reactive bulk compositions from this study have lower FeO content as magnetite and ilmenite were omitted from the reactive rock composition calculations.

	Measured XRF Sossi et al., 2016	H_2O only This study	$XCO_2 = 0.1$ This study
SiO_2	37.6	39.6	36.8
Al_2O_3	2.1	2.3	2.1
FeO	8	4.8	4.4
MgO	31.5	29.8	27.7
CaO	6.2	7.1	6.6
H_2O	14.6	16.5	19.5
CO_2	–	–	2.2
X_{Mg}	0.79	0.86	0.86
XCO_2	–	–	0.10

3.2. Phase equilibria modelling

The representative komatiite B331-783 was modelled with Perple_X (Connolly, 2009) with the updated Holland and Powell (2011) dataset 6 (file: hp622ver.dat) to model fluid release during prograde metamorphism, in both CO_2-free and CO_2-bearing scenarios. In the CO_2-free calculation the chemical system is SiO_2-Al_2O_3-FeO-MgO-CaO-H_2O (CFMASH), water (H_2O) is a pure phase and was included in high enough contents to saturate the mineral assemblages at greenschist facies conditions ($\sim$ 300 °C; Table 1), which also matched the reactive rock composition estimate at approximately 6 wt.% (Fig. 3b). A CO_2-bearing calculation was also undertaken to assess the effect of carbonate formation and CO_2 release on predicted mineral assemblages and dehydration reactions, using the same representative komatiite starting chemistry and in the same chemical system + CO_2. The fluid was considered in a binary CO_2-H_2O system; the composition used (Table 1) corresponds to a molar X_{CO2} ($X_{CO2} = CO_2/(CO_2+H_2O)$) of 0.1, or $\sim$2 wt.% CO_2. This value was obtained from the geochemical database as the mean of 1770 whole rock analyses (Supp. Fig. 1). Solution models used in the phase equilibria modelling are in Supplementary Table 1.

The representative reactive rock composition for sample B331-783 was calculated using quantitative EPMA maps and mineral proportions in the program XMapTools (Table 1; Fig. 4; Lanari et al., 2014, 2019). The reactive rock composition incorporated large areas of antigorite and chlorite-rich spinifex olivine pseudomorphs and chlorite and tremolite-rich matrix (Fig. 3a). Magnetite, ilmenite and titanite were not included in the reactive rock composition. Firstly, magnetite is interpreted to form early in the alteration history of the komatiites, most likely during low-temperature serpentinisation, sequestering Fe from the rock system and remaining mostly unreactive during further metamorphism (e.g. Bretscher et al., 2018; Vieira Duarte et al., 2021). Secondly, magnetite contains significant Fe^{3+}, and as such Fe_2O_3 would need to be included in the compositional system. This requires that the amount of Fe^{3+} in chlorite, antigorite and amphibole is estimated from EPMA data, which introduces a significant uncertainty into the bulk rock Fe^{3+}. Including magnetite, ilmenite and titanite also would require Cr_2O_3 and TiO_2 to be considered in the compositional system, introducing similar difficulties with the silicate solution models, which do not contain these components, resulting in the stability of these minerals possibly being overestimated. When Fe_2O_3 and magnetite are included in the phase equilibria modelling, the composition of magnetite is incorrectly predicted (due to Cr_2O_3 being omitted from the system), however the stability fields of chlorite, antigorite and tremolite remain similar. As such, omitting magnetite, ilmenite and titanite from the phase equilibria modelling has little effect on the modelled stability of the silicate minerals (e.g., Bretscher et al., 2018). Therefore, the calculated reactive rock composition X_{Mg} is

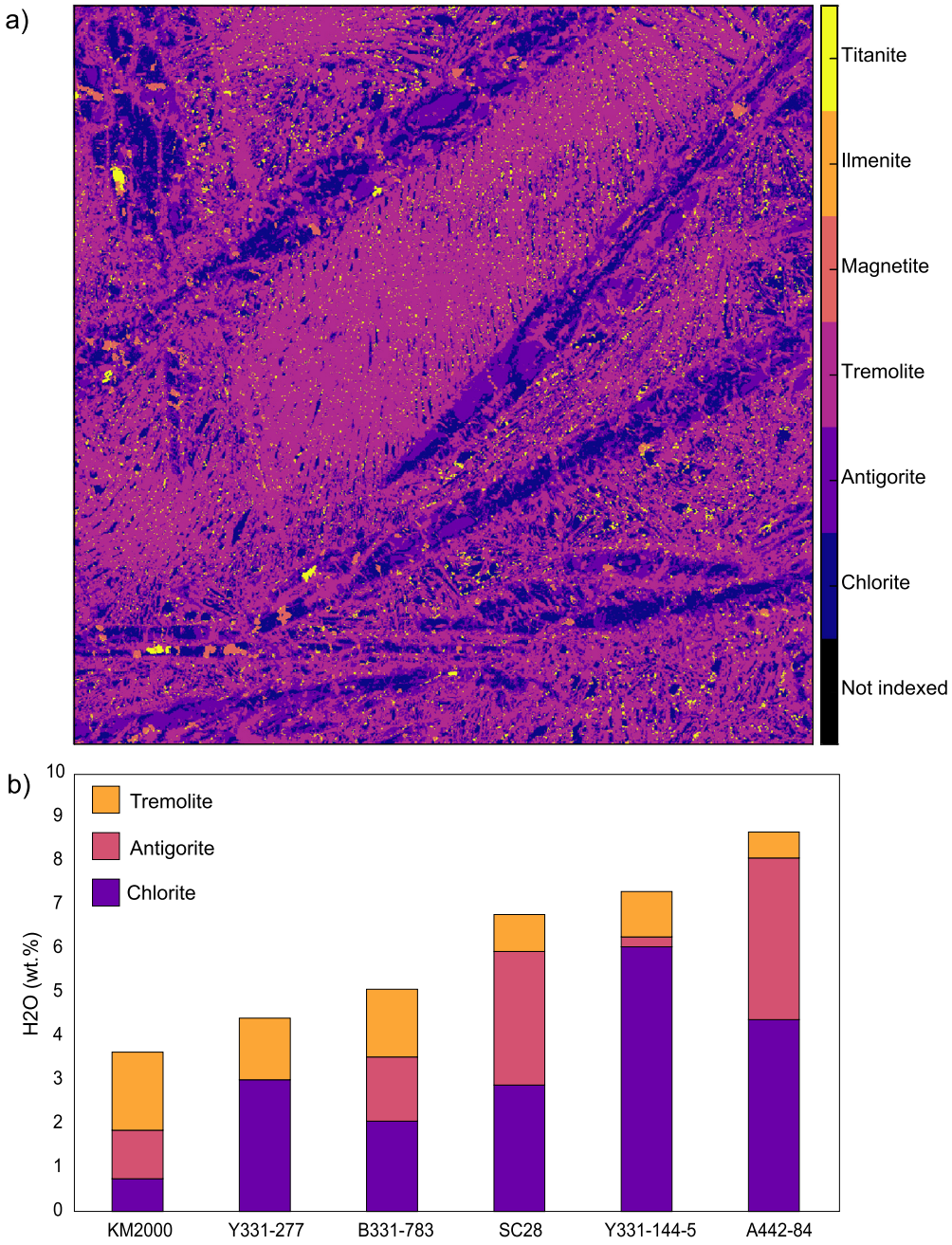

Fig. 3. **(a)** Phase map of komatiite sample B331-783, constructed from EPMA maps using the program XMapTools (Lanari et al., 2019). **(b)** Cumulative water budget in six komatiite samples, modal proportions were also calculated from EPMA maps and XMapTools (Lanari et al., 2019). At greenschist-amphibolite facies conditions, water is held in chlorite, antigorite and tremolite, however chlorite is the most effective reservoir as it has high water content and can persist to high temperatures.

0.86, closer to the X_{Mg} of silicate minerals in the sample, which have an average X_{Mg} of 0.89 (Fig. 4). The slightly lower X_{Mg} of the reactive rock composition compared with the silicate minerals is due to the EPMA mapping process; analyses containing a mixed signal between amphibole and fine-grained magnetite were incorporated into the map and the reactive rock composition calculation (Fig. 3).

3.3. Database analysis

To complement the petrological study of the representative komatiite, bulk geochemical analyses of komatiites and basaltic komatiites from a geochemical database (updated from Gard et al., 2019; Supp. Table 2) were investigated. In particular, the relationships between X_{Mg}, Al_2O_3, CaO and LOI (loss on ignition) were of interest. Komatiites and basaltic komatiites were filtered for by bulk rock chemistry, age, and geographical location. The parameters used to filter the database were (i) analyses plot in the komatiite and basaltic komatiite field of Jensen diagram (Jensen et al., 1976) and (ii) analyses must be Archean in age, or in the absence of an age, their location must fall within an Archean craton or reworked Archean craton (Fig. 1; Hasterok et al., 2022).

4. Results

4.1. Mineral compositions

The compositions of antigorite, chlorite, and tremolite were measured across the five komatiite samples, including the representative komatiite chosen for mineral equilibria modelling, and

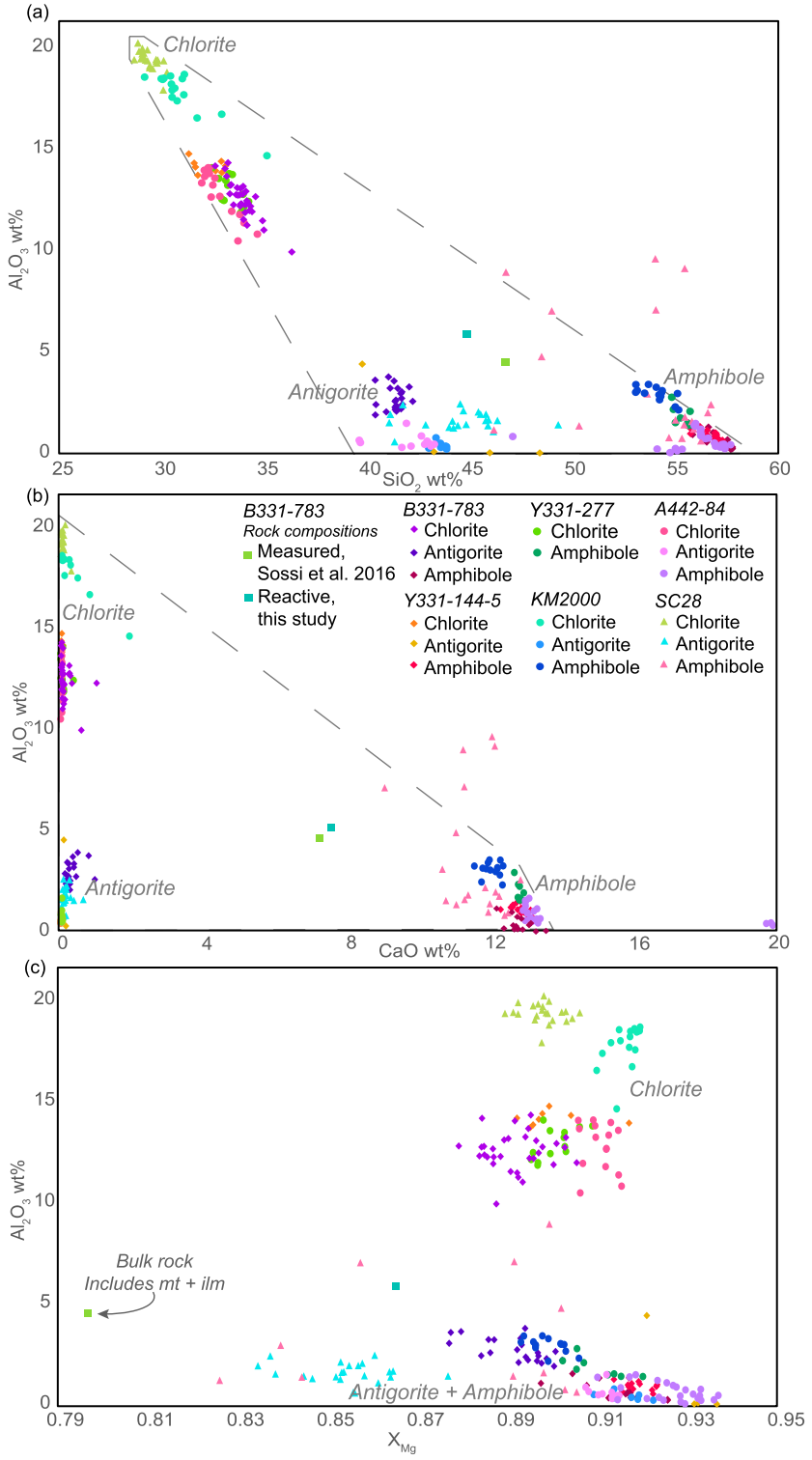

Fig. 4. Silicate mineral chemistry of representative metamorphosed komatiites, grey dashed lines indicate the compositional boundaries defined by the mineral compositions. Mineral compositions are similar across the komatiite and basaltic komatiite compositions, however chlorite forms a high Al_2O_3 and a low Al_2O_3 group. Square symbols denote rock compositions for representative komatiite B331-783. **(a)** Al_2O_3 vs SiO_2. **(b)** Al_2O_3 vs CaO. **(c)** Al_2O_3 vs X_{Mg}, showing systematically high X_{Mg} for antigorite, chlorite and amphibole, with the exception of basaltic komatiite sample SC28. There is a notable difference in bulk rock X_{Mg}, which includes oxide minerals, and the reactive rock X_{Mg}, calculated from XMapTools by excluding magnetite and ilmenite.

one basaltic komatiite (Fig. 4; Supp. Table 3), from four Archean greenstone belts (Fig. 1). These mineral compositions are presented to assess the representability of the mineralogy of Barberton sample (B331-783), and to investigate the reactive X_{Mg} of komatiites from different localities.

Chlorite from B331-783 is dominantly clinochlore (X_{Mg} = 0.89–0.90), and 0.10–0.12 proportion daphnite, with SiO_2 of between 32–36 wt.% (3.18–3.50 Si a.p.f.u.) and 10–15 wt.% Al_2O_3 (1.13–1.56 Al a.p.f.u.; Supp. Table 3). Similarly, chlorite from all other komatiite samples show high SiO_2 and low Al_2O_3 contents

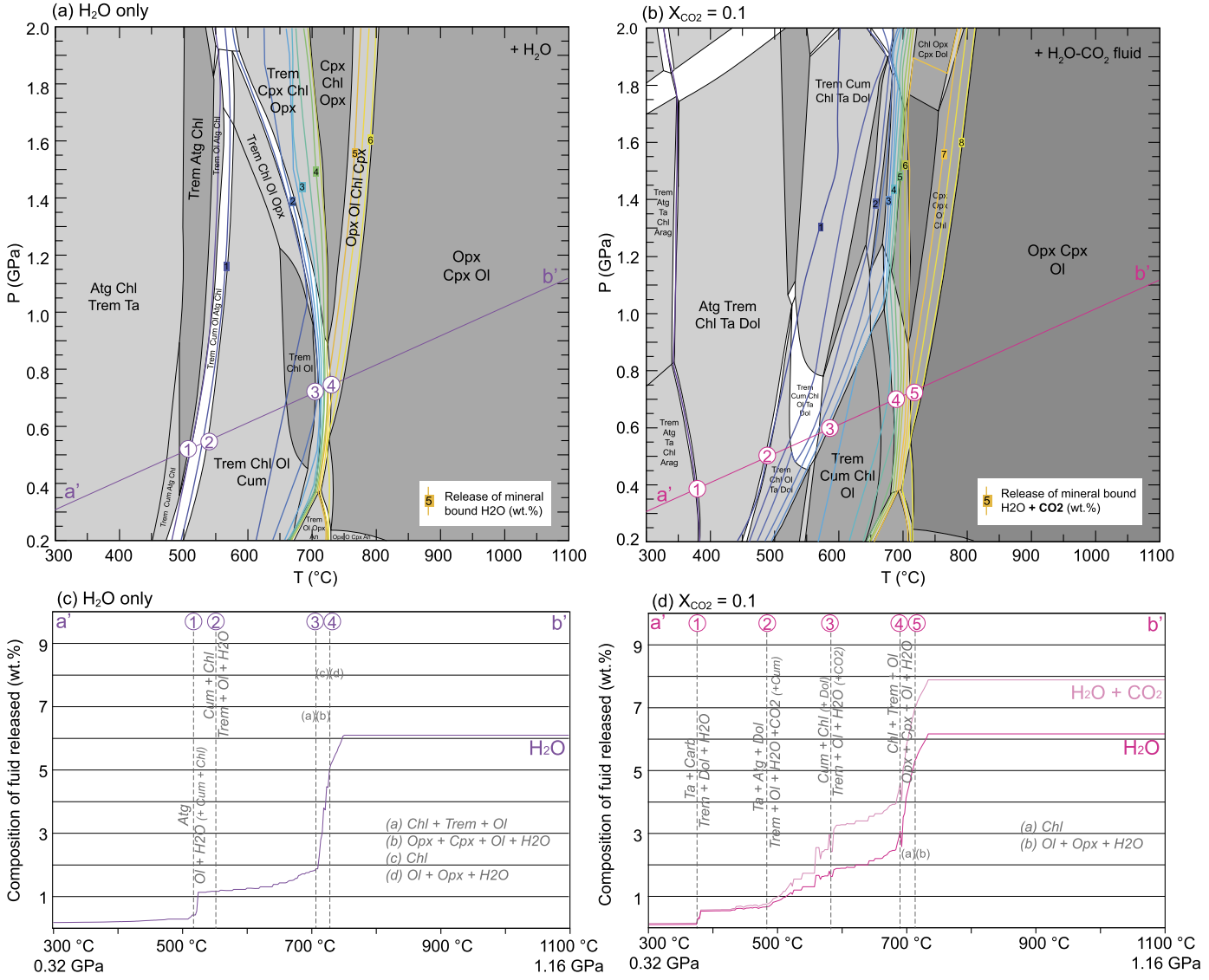

Fig. 5. Results of phase equilibria modelling of representative komatiite B331-783. **(a)** Model containing H_2O fluid only, with H_2O release contours. **(b)** Model containing a binary H_2O-CO_2 fluid and an XCO_2 of 0.1, with fluid release contours. **(c)** Dehydration reactions and fluid release across a thermal gradient of 950 °C/GPa for the H_2O diagram. **(d)** Dehydration and decarbonation reactions across the same thermal gradient in the H_2O-CO_2 system. Atg: Antigorite, Chl: Chlorite, Cum: Cummingtonite, Trem: Tremolite, Ta: Talc, Ol: Olivine, Cpx: Clinopyroxene, Opx: Orthopyroxene, An: Anorthite. Carb: Ca-Mg carbonate, Dol: Dolomite, Arag: Aragonite.

(Fig. 4a), with X_{Mg} ranging between 0.87–0.92 (Fig. 4c; Supp. Table 3). An exception is chlorite from the basaltic komatiite (SC28) and one komatiite from the Komati formation (KM2000), which have slightly higher Al_2O_3 content, up to 20 wt.%, but identical X_{Mg}.

Antigorite from B331-783 consistently contains FeO_{tot} contents of 6.5–6.9 wt.%, and 1.9–2.6 wt.% Al_2O_3, with an X_{Mg} of ~0.89. Antigorite from the other komatiite samples generally has between 4.8–6.4 wt.% FeO_{tot} (X_{Mg} = 0.88–0.94), except for the basaltic komatiite which contains between 8.6–11.1 wt.% FeO_{tot}, resulting in scattered X_{Mg} between 0.83 and 0.88. Al_2O_3 content in antigorite across all samples reaches up to 4.4 wt.% (Fig. 4).

Amphibole from all samples is tremolitic in composition, with X_{Mg} of 0.89 to 0.94 (Fig. 4b,c). Amphibole from B331-783 falls in the centre of this range with an X_{Mg} of ~0.92. Again, the exception is the basaltic komatiite, with lower X_{Mg} in the range of 0.83 to 0.88.

4.2. Phase equilibria forward modelling

Results of the Perple_X phase equilibria forward modelling in the CO_2-free system predicts expected mineral assemblages in sample B331-783, and matches those observed in the greenschist and lower amphibolite facies komatiites presented in this study: primarily tremolitic clinoamphibole, antigorite, and chlorite (Fig. 5a). The key dehydration reactions which take place between 0.2–2 GPa are outlined in Fig. 5c and are as follows:

1. Antigorite out at 450 to 550 °C, by reaction to olivine, cummingtonite, chlorite and H_2O (Atg → Ol + Cum + Chl + H_2O). This reaction releases approximately 1 wt.% H_2O.
2. At lower pressures (<1.2 GPa), continuous breakdown of cummintonite and minor amounts of chlorite to produce olivine, tremolite and H_2O from 500 to 700 °C, releasing up to 1 wt.% H_2O (Chl + Cum → Ol + Trem + H_2O).
3. Tremolite, olivine and partial chlorite breakdown between 600 to 720 °C by reaction to orthopyroxene, clinopyroxene and H_2O (Trem + Chl + Ol → Opx + Cpx + H_2O). This reaction is the terminal tremolite breakdown. Above 1.2 GPa this reaction releases 3.5 wt.% H_2O, below 1.2 GPa it releases 2.5 wt.% H_2O.
4. Terminal chlorite breakdown at temperatures between 700 and 800 °C (Chl → Ol + Opx + H_2O + *Sp*). Spinel (*Sp*) was

not stabilised in the phase diagram due to the reduced compositional system used but is likely to balance this reaction for Al_2O_3 in nature. This reaction releases a further 1 wt.% H_2O.

These dehydration reactions release a total of 6 wt.% H_2O over a temperature range of ~ 500 to 800 °C (Fig. 5a). The primary contributor is chlorite, which contains 50% of the mineral-bound H_2O in the rock, comparable with other investigated samples in this study (Fig. 3). Along a P–T transect following an average Archean thermal gradient of 950 °C/GPa (Brown and Johnson, 2018), just over 4 wt% of the H_2O is effectively released over a small temperature range of 700 to 800 °C (Fig. 5c). Talc is also present in the model, but in low abundance (<2.5 vol.%), and therefore does not contribute significantly to the dehydration reactions in this compositional space. However, in more Si-rich compositions, talc may also play an important role in dehydration reactions at lower temperature conditions (e.g., Spandler et al., 2008). Additionally, orthoamphiboles and zoisite (or clinozoisite/epidote) were not predicted to be stable in the selected composition but could be important for dehydration in other komatiite and basaltic komatiite compositions. Cummingtonite has not been identified in the representative komatiite samples, though it is present in low abundance (<2 vol.%) in the phase diagram at lower pressure conditions.

The computed modal abundances of antigorite, chlorite, and amphibole are similar to those observed in sample B331-783, however do not converge at a common pressure-temperature conditions (Supp. Fig. 2). This is possibly due to the poorly predicted Al_2O_3 content of modelled chlorite (e.g., Kempf et al., 2022). Chlorite from B331-783 and other analysed komatiites is dominantly pennine, with Al_2O_3 content as low as 10 wt.% (Fig. 4). Al_2O_3 content in modelled chlorite is clinochlore that ranges between 17 and 19 wt.% across the entire phase equilibria diagram (Supp. Fig. 2). Modelled chlorite SiO_2 content is correspondingly underestimated, ranging between 30.8–32.5 wt.%, versus measured SiO2 concentrations of between 32–35 wt.% (Supp. Fig. 2). X_{Mg} of modelled olivine is between 0.55 and 0.6 at the olivine-in reaction, when natural metamorphic olivine in equilibrium with high X_{Mg} silicates generally has a higher X_{Mg} of >0.7 (Kempf et al., 2022).

Modelled X_{Mg} values for tremolite, antigorite, and chlorite match the measured data from the representative komatiite well (Supp. Fig. 2). In modelled tremolite the X_{Mg} reaches 0.89, X_{Mg} in measured tremolite from B331-783 is generally higher, and ranges from 0.89 to 0.92. Modelled chlorite X_{Mg} lies between 0.70 and 0.89, and natural chlorite overlaps with the upper end of this range at 0.87 to 0.91. X_{Mg} of modelled antigorite ranges from 0.87 to 0.91, which matches measured antigorite perfectly, with an X_{Mg} of 0.87 to 0.91. This confirmation of well-matched X_{Mg} across the phases suggests that the inclusion of mixed magnetite and amphibole in the calculated reactive rock composition was only minor, and did not significantly affect the X_{Mg} of the modelled phases.

Phase equilibria modelling with an X_{CO2} of 0.1 (Fig. 5b) predicts mineral assemblages and compositions similar to those of H_2O only, except for addition of pure calcite/aragonite, pure dolomite, and a carbonate with Ca-Mg solid solution. This diagram is susceptible to the same issues described for the H_2O-only calculations, such as the poorly predicted Al_2O_3 and SiO_2 content in chlorite. The key dehydration-decarbonation reactions between 0.2–2.0 GPa are as follows, illustrated in Fig. 5d:

1. Talc and Ca-carbonate react to tremolite, pure dolomite and H_2O at temperatures less than 400 °C, releasing 0.5 wt.% H_2O (Ta + Carb → Trem + Dol + H_2O).
2. Talc, antigorite and dolomite react to tremolite, olivine, H_2O, CO_2 and minor cummingtonite (Ta + Atg + Dol → Trem + Ol + Cum + H_2O + CO_2), between temperatures of 450 °C to 680 °C depending on pressure. This releases approximately 1.3 wt.% H_2O and 1.5 wt.% CO_2. Talc and antigorite are exhausted by this reaction.
3. Cummingtonite, chlorite and minor dolomite continuously react to tremolite, olivine, H_2O and CO_2 between temperatures of 580 to 660 °C depending on pressure, releasing 1.2 wt.% H_2O and approximately 0.5 wt.% CO_2 (Cum + Chl + Dol → Trem + Ol + H_2O + CO_2). Dolomite stability persists to temperatures of 720 to 800 °C at pressures above 1 GPa, and this is the terminal carbonate breakdown reaction.
4. Tremolite, chlorite and olivine breakdown between 650 to 710 °C by reaction to orthopyroxene, clinopyroxene and H_2O, releasing approximately 2 wt.% H_2O (Trem + Chl + Ol → Opx + Cpx + H_2O). Tremolite is exhausted by this reaction.
5. Terminal chlorite breakdown at temperatures between 700 and 810 °C (Chl → Ol + Opx + H_2O + *Sp*). Spinel (*Sp*) was not stabilised in the phase diagram due to the reduced compositional system used, but is likely necessary to balance this reaction for Al_2O_3. This reaction releases a further 1 wt.% H_2O.

Reaction 2 and 3 are the decarbonation reactions. They have a positive slope in P–T space, but most CO_2 is released below 500 °C at 0.2 GPa and below 700 °C at 1.8 Gpa. The low temperature dehydration reactions are therefore influenced by the carbonate equilibria. Talc is stabilised in higher proportions than the H_2O-only diagram and partially dehydrates at ~370 °C (reaction 1) and terminally along with antigorite at 460 to 680 °C, collectively releasing ~3 wt% H_2O. The final chlorite and tremolite breakdown reactions are the same as those in the H_2O-only diagram, but they release slightly less water (1 wt% less) and occur at slightly lower temperatures because the modal proportion of chlorite is lower (Fig. 5c, d).

The X_{Mg} of modelled silicate phases in the CO_2-bearing calculation are generally lower than those in the CO_2-free calculation, but only when dolomite is present, as dolomite sequesters Mg. When dolomite is destabilised via reactions 2 and 3, the X_{Mg} of tremolite and chlorite increases up to 0.93 and 0.94 respectively, comparable with the CO_2-free phase equilibria model.

4.3. Database analysis

The global database contains 3206 analyses of komatiite and 5501 analyses of basaltic komatiite, with a total of 8707 data (Fig. 1; 6). However, there are only 1911 komatiite analyses with LOI and 3678 basaltic komatiites analyses with LOI, leaving a total of 5589 data. Two thirds of komatiites are Archean in age, however half of basaltic komatiites are Archean and half are from reworked Archean crust (approx. 2.5–2.35 Ga; Fig. 6b). We investigate LOI as a proxy for degree of hydration, with the caveat that the LOI represents the sum of all volatiles in the whole rock (H_2O, CO_2) as discussed below.

Before interpreting the results of the database analysis, it is important to discuss the possible biases or problems which may be associated with the dataset. Sampling bias is the most prevalent. While almost all komatiites in the geological record are altered, it is most likely that less-altered samples are usually chosen by geologists when sampling in the field, as most komatiites and komatiitic basalts are studied for their magmatic and eruptive histories. Carbonate-bearing samples are not likely to be chosen during sampling for geochemical analysis, so a low-CO_2 sampling bias is possibly introduced to the dataset. An observational bias stems from the use of LOI. While LOI is a useful proxy for degree of hydration of these originally anhydrous rock types, it combines H_2O (degree of hydration), CO_2 (degree of carbonation) and other minor volatiles into one single parameter. Evidence for carbonated samples is clear from elevated CaO and depressed MgO content at LOI values in excess of ~12 wt.% (Supp. Fig. 3), as calcite is a

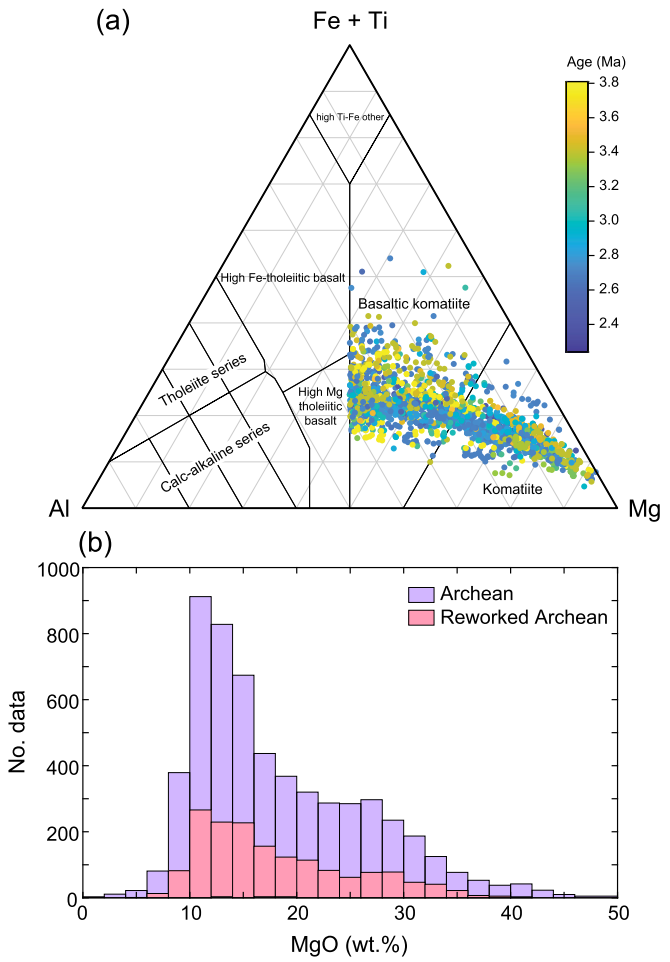

Fig. 6. Chemical composition of komatiites and basaltic komatiites in the dataset. **(a)** Jensen plot used to discriminate komatiite and basaltic komatiites in the dataset (Fig. 1), with data colour-coded for approximate crystallisation age. If no age was available in the dataset the nearest geological age was applied, this is an approximation but necessary due to the difficulties in obtaining ages from komatiitic rock compositions. **(b)** Cumulative number of komatiite and basaltic komatiite data in Archean and reworked Archean crust, and total data points in the dataset. A bimodal distribution can be seen in the data, with komatiites defining the high (~28 wt. %) MgO peak and basaltic komatiites defining the lower (~12 wt. %) MgO peak.

primary CO_2 bearing phase. However, as we are focused on samples with LOI values below 12 wt.%, we suggest that LOI below this value primarily represents the H_2O content. This assumption is supported by the fact that measured CO_2 values from the database are very low (Supp. Fig. 1), with a median value of only 0.33 wt.%. It is also supported by the normal distribution of LOI content in komatiite data, with a mean of 6 wt.% (Fig. 7a), identical to the water content estimated from phase equilibria forward modelling (Fig. 5) and similar to the water content calculated from representative komatiites in this study (Fig. 3). For the 408 samples that contain measured H_2O data, the mean is 6.2 wt.%.

In Fig. 8, whole rock SiO_2, CaO, X_{Mg} vs. Al_2O_3 from all komatiites and basaltic komatiites from the dataset are presented, coloured by LOI. Compositions of representative antigorite, chlorite and tremolite are also shown for comparison (Fig. 4), the compositional boundaries, i.e., the field defined by mixing between these phases, is outlined by dashed lines. LOI increases with decreasing SiO_2 and Al_2O_3, as the modal proportion of antigorite increases and that of amphibole decreases (Fig. 8a). In the CaO vs Al_2O_3 plot, the LOI of komatiitic samples are negatively correlated with CaO and Al_2O_3 content, as the increasing LOI is controlled by the mode of antigorite and/or chlorite in the sample (Fig. 8b). The relationship between CaO, Al_2O_3, and LOI can be fit by a plane (colour contours), with the relationship LOI (wt.%) = 10.56 – 0.43 CaO (wt.%) – 0.32 Al_2O_3 (wt.%; Fig. 8b). This relationship is defined by approximately 95% of the data with a misfit of 2%, the omitted 5% of the data were deemed as outliers, exceeding 4.1 times the mean Cook distance (Cook, 1997). A strong relationship between X_{Mg} and LOI is also evident (Fig. 8c), LOI increases with bulk rock X_{Mg} (in this case, X_{Mg} = Mg/(Mg+Fe_{tot}), with a shift to LOI values of >6 wt.% at an X_{Mg} of 0.8 and higher. We note, however, that these bulk rock data include magnetite, which we interpret to be mostly unreactive during metamorphism of komatiitic compositions. Consequently, the bulk rock X_{Mg} is not representative of the reactive rock composition, and therefore does not necessarily correlate with the X_{Mg} of the representative silicate phases.

To further investigate the relationship between LOI and bulk rock X_{Mg} in komatiites and basaltic komatiites, the mean of the LOI in the bulk rock data was taken for X_{Mg} bins of 0.2 (Fig. 7a). The result shows a semi-exponential relationship between bulk rock X_{Mg} and LOI. The highest mean LOI is 9.5 wt.% for an X_{Mg} of 0.9; however, there are low numbers of data in this bin (Fig. 7b). Komatiite analyses have a nearly normal distribution in LOI (yellow bars in Fig. 7b) with a mean of 6 wt.% (dashed line in Fig. 7b), basaltic komatiites skew to lower values with a mean of only 3 wt.% LOI (Fig. 7b).

5. Discussion

5.1. All komatiites are hydrated

A well-described but perhaps underappreciated fact is that all ancient komatiites are extensively hydrated (Arndt, 2003). This hydration most likely occurs in an Archean ocean, as most komatiites are interpreted as submarine eruptions. Evidence for komatiite eruption underwater can be found as trapped vesicles within the crystallised lavas (Dann, 2000) and pillow structures, reported from both komatiites and basaltic komatiites (Arndt et al., 2008). Komatiites are also often associated with other submarine rock types, such as carbonates, banded iron formations and shales, and submarine microbial mats (e.g., Homann, 2019). From this evidence it appears that komatiites undergo a similar process to that which is observed at present-day MORs, where erupted mafic rocks are altered at low temperature conditions.

The exact volume and stratigraphic distribution of komatiites in Archean terranes is difficult to constrain, due to limited or poor outcrop, deformation and metamorphism. One estimate of the volume of komatiite in a greenstone belt is from Dann (2000), who estimated that 50% of the Komati Formation and 28% of the Barberton Greenstone Belt, in the area that was mapped, is comprised of komatiite. Additionally, the stratigraphic thickness of individual komatiite flows can range from less than 50 centimetres to more than 500 meters (Arndt et al., 2008). The original spatial extent of komatiite formations is unknown, however the surviving areal extent of individual komatiite flows are estimated to have been at least 85 to 700 kilometers in diameter (Arndt et al., 2008). Considering the extreme hydration potential of komatiitic rock compositions, their occurrence in all greenstone belts worldwide, and their potential volume, komatiites could have been responsible for the fixation of vast quantities of H_2O in the Archean.

5.2. Mineralogical control on H_2O contents and retention in altered komatiites

The low SiO_2 + CaO and high X_{Mg} nature of komatiites directly controls their hydration potential during low temperature seafloor alteration. As the majority of komatiites and associated basaltic rocks are now metamorphosed to greenschist-amphibole facies, the

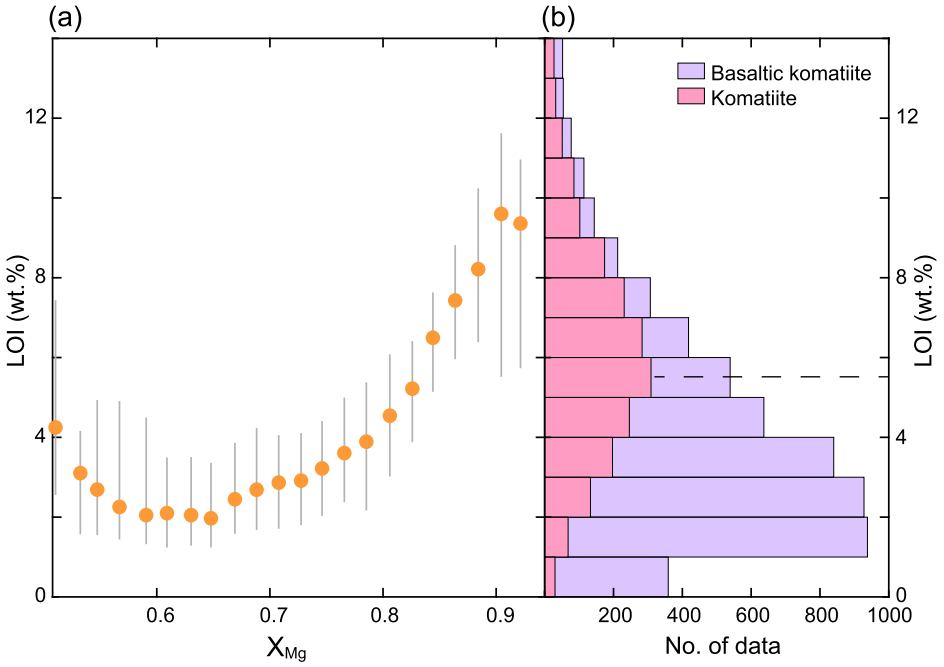

Fig. 7. Mean X_{Mg} vs LOI for komatiites and basaltic komatiites in the dataset (n = 5589). Data is binned by X_{Mg} steps of 0.1, grey bars indicate the interquartile range of the data. The high X_{Mg} (>0.84) samples are likely dominated by olivine cumulates, or have undergone metasomatism. **(b)** Cumulative number of data for each 1 wt.% step LOI. The komatiite only dataset averages 6 wt.% LOI (dotted line), however the data for the basaltic komatiites is clustered at approximately 2 wt.% LOI.

LOI of these samples possibly reflects some loss of volatiles during low-grade metamorphism relative to their initial hydration. However, the difference in extent of hydration between komatiite to more basaltic compositions is still evident (Fig. 7; 8), despite their variable metamorphic overprints. During alteration of komatiites, the low bulk SiO_2/MgO ratio and generally high X_{Mg} result in formation of serpentine minerals, which contain up to 13 wt.% H_2O in their crystal structure. Low SiO_2 and CaO contents of the komatiites promote the formation of chlorite and antigorite at the expense of amphiboles during low-grade metamorphism. Tremolite is stable, and the majority of the Al_2O_3 budget of the rock is sequestered into high X_{Mg} chlorite. In the presented dataset, the bulk Al_2O_3 content appears to have a secondary control on the bulk rock LOI (Fig. 8). High Al_2O_3 komatiites likely have higher proportions of chlorite, whereas low Al_2O_3 komatiites likely have higher proportions of antigorite. As both chlorite and antigorite contain approximately 13 wt.% H_2O, varying bulk Al_2O_3 content does not have a strong control on bulk H_2O and therefore LOI at greenschist- to lower amphibole-facies conditions where antigorite and chlorite coexist. However, the role of Al_2O_3, and also X_{Mg}, is important after antigorite breakdown at temperatures between ~ 480 and 550 °C. At these higher grades, Al_2O_3 content determines chlorite mode, which in turn dictates the fraction of lattice-bound H_2O in the rock, and the high rock X_{Mg} promotes formation of Mg-rich chlorite, which remains stable to ~800 °C (Fig. 9). Therefore, Al-enriched and Al-undepleted komatiites will transport more H_2O to greater depths than Al-depleted komatiites, highlighting the role of primary komatiite composition in water transport and release in the Archean Earth.

During serpentinisation and metamorphism komatiites produce silicate minerals with extremely high X_{Mg}. This is due to their highly magnesian starting compositions (>18 wt% MgO), but is strongly enhanced by the formation of magnetite during ocean-floor serpentinisation, which sequesters Fe from former magmatic minerals. In ultramafic rocks, early-formed magnetite remains mostly unreactive during metamorphism, it is not broken down and can even be produced when minor amounts of Fe^{3+} are liberated from the breakdown of antigorite and chlorite (Bretscher et al., 2018; Evans and Frost, 2021; Vieira Duarte et al., 2021). Therefore, silicate minerals with high X_{Mg} form, which can remain stable to higher temperatures than their Fe-rich counterparts. For example, in ultramafic compositions Mg-rich chlorite (X_{Mg}= ~0.94) can persist to temperatures of ~ 850 °C at pressures of 2 GPa (Fig. 9; Staudigel and Schreyer, 1977; Spandler et al., 2008; Lakey and Hermann, 2022), and pure clinochlore may persist up to ~880 °C at pressures of 1.6 GPa (Jenkins, 1981). This extreme hydration potential combined with the stability of the hydrous mineral chlorite to very high temperatures, and the fact that no fresh komatiite exists in the Archean geological record, all suggests that komatiites were a key player in the water budget and cycling in the early Earth.

5.3. Komatiites can transport and release water into the crust to form TTGs

The estimation from phase equilibria modelling that komatiites can transport 6 wt.% water (or approximately 20 vol.% H_2O) to crustal conditions of 500–800 °C is a minimum estimate for sample B331-783. Al_2O_3 and SiO_2 content of modelled chlorite is overestimated, therefore modelled chlorite mode (and hence the amount of water released) is underestimated. This, in addition to the underestimated X_{Mg} of olivine, likely expands the stability field of hydrous minerals to higher temperatures in nature, in favour for flux melting of associated metabasalts.

To understand the effect of water release by komatiites during metamorphism, water release contours from the phase equilibria modelling are shown in Fig. 9, with several other key geological data. Pressure-temperature data points of metamorphic rocks from the Archean are shown (Brown and Johnson, 2018), as well as minimum, mean and maximum thermal gradients recorded by these metamorphic samples. These data fall between thermal gradients of 15 °C/km^{-1} to 50 °C/km^{-1}, and do not exceed 1.5 GPa (Fig. 9; approximately 45 km), pointing to the most likely crustal thickness at this time, or at least the greatest depth which metamorphic rocks were exhumed from. Regardless of the style of plate tectonics operating in the Archean, these data are meaningful representations of the conditions experienced and preserved by then-existing

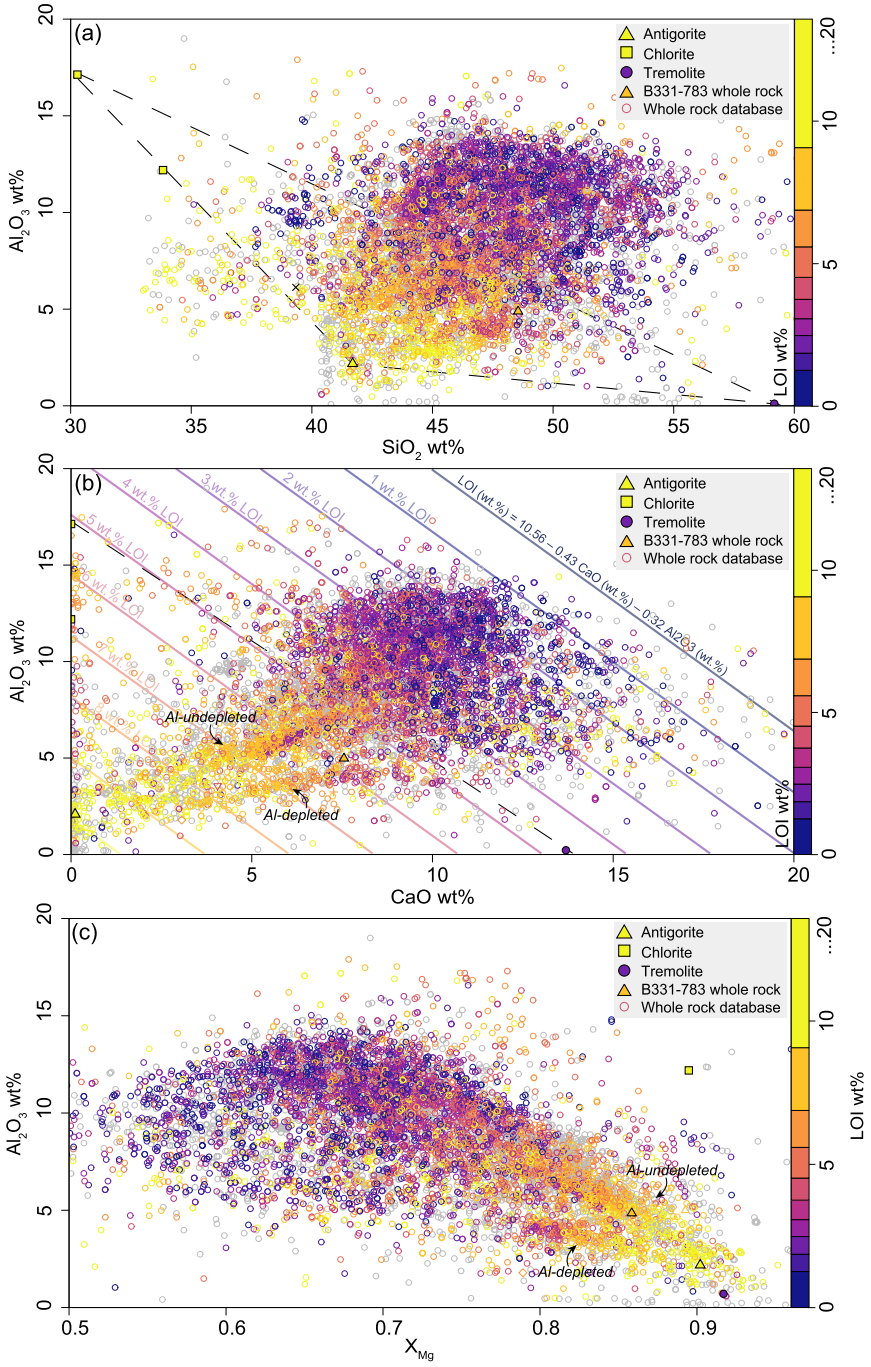

Fig. 8. Geochemical plots of komatiites and basaltic komatiites from the dataset, colour coded for LOI value. Grey analyses do not have an LOI value. Representative mineral compositions of chlorite, antigorite, and tremolite are plotted for comparison, grey dashed areas represent the range of bulk rock compositions (minus Fe-bearing oxides such as magnetite, ilmenite and hematite) represented by these mineral compositions. Note that the data are not normalised to an anhydrous composition. Al-undepleted and Al-depleted komatiite groups can be discerned in two linear trends in the data. **(a)** Al_2O_3 vs SiO_2. **(b)** Al_2O_3 vs CaO. The data can be fit by a plane (colour contours), LOI (wt.%) = 10.56 – 0.43 CaO (wt.%) – 0.32 Al_2O_3 (wt.%) with a misfit of 2.0 wt.%, contours for the best fit plane are coloured by LOI value. Approximately 95% (5324/5589) of the initial data are used to fit the plane. **(c)** Al_2O_3 vs X_{Mg}, note that X_{Mg} is Mg/(Mg+Fe_{total}).

crust and, therefore, constrain the likely thermal gradients experienced by hydrated komatiites when they were metamorphosed. The experimentally-constrained wet basalt solidus is shown (Fig. 9; Lambert and Wyllie, 1972), and its location in P–T space is supported by other experimental data (Rapp et al., 1991; Rapp and Watson, 1995; Zhang et al., 2013), as well as the solidus for amphibole dehydration melting (Green, 1976; Wyllie and Wolf, 1993). Within the probable pressure ranges of metamorphism of komatiites in the Archean (0.4–1.6 Gpa), the dehydration reactions involving antigorite breakdown release ∼ 1 wt.% H_2O from 500 to 600 °C, below the wet basalt solidus. Above the wet basalt solidus, tremolite and chlorite breakdown release a further 5 wt.% H_2O across a temperature range of 670 to 800 °C (Figs. 5, 9), comparable with estimates of water release from metamorphosed komatiites from Hartnady et al. (2022) of approximately 20 vol.%. The experimental constraints of Mg-chlorite breakdown are also shown, to represent the maximum thermal stability of chlorite (Staudigel and Schreyer, 1977; Jenkins, 1981; Lakey and Hermann, 2022).

Based on the analysis above, komatiite dehydration appears to be a very likely source of free water for wet basalt melting to

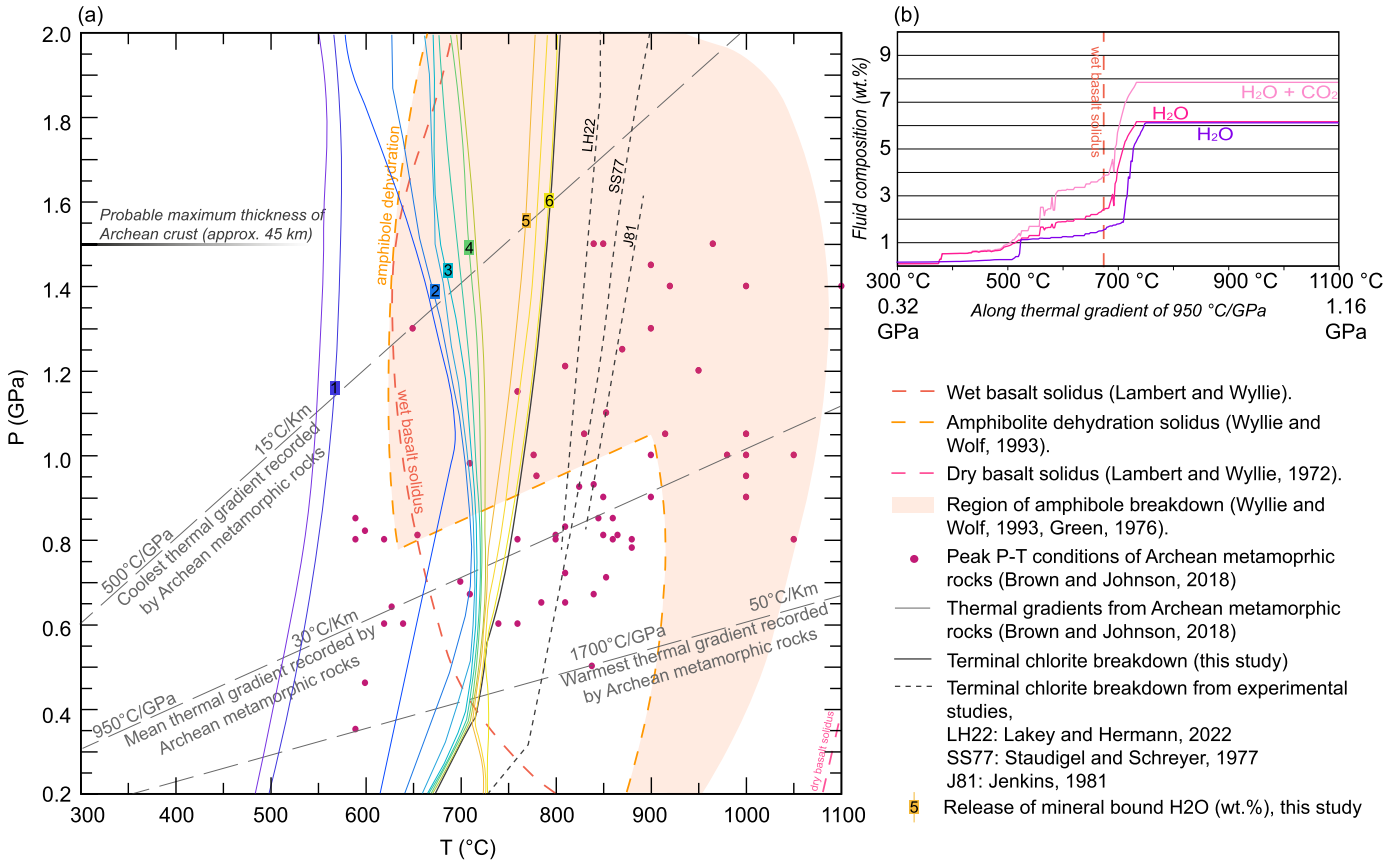

Fig. 9. Summary of data from phase equilibria modelling and the literature, suggesting the likely pressure-temperature conditions of komatiite dehydration and wet basalt melting. **(a)** P–T diagram showing key dehydration contours (i.e., the mass of water released) from the H_2O-only phase equilibria model, with the experimental wet basalt solidus. Grey dashed lines indicate the range of likely thermal gradients in the Archean, from metamorphic T/P data, 950 °C/GPa is the mean thermal gradient. Experimental chlorite-out lines are from LH22: Lakey and Hermann (2022), SS77: Staudigel and Schreyer (1981), J81: Jenkins (1981). **(b)** Compiled H_2O and CO_2 release along the 950 °C/GPa thermal gradient from the two-phase equilibria models, both showing significant water release above the wet basalt solidus.

form TTGs in the Archean. The temperature range of tremolite and chlorite breakdown in komatiite (670–800 °C) overlaps with the lower end of the range in Ti saturation temperatures of Archean TTGs (750–950 °C; Xiong et al., 2009). These temperatures are estimated at pressures of 1.5 and 2.5 GPa, however, Ti saturation temperature estimates below 1.5 GPa are unlikely to be significantly different (Xiong et al., 2009). These temperature estimates are supported by wet basalt melting experiments, where water is present as a free phase, which show that partial melt volumes of 10–40% at 800–950 °C have TTG compositions (Qian and Hermann, 2013). Numerous studies using phase equilibria forward modelling to predict melt compositions during wet basalt melting also show that temperatures between 750–950 °C and high (>1 wt.%) water contents are necessary to create TTG melts (e.g. Johnson et al., 2017; Pourteau et al., 2020). Considering that komatiite dehydration occurs within the lower portion of the 750–950 °C temperature range for basalt melting, we suggest that the dehydration reactions within komatiite triggers initial basalt melting, which in some situations can continue melting with increasing temperature to form higher-temperature tonalites.

The effect of CO_2 on the modelled phase equilibria and dehydration reactions for a XCO_2 of 0.1 is minimal when compared to the pure water system. The XCO_2 of 0.1 was chosen from the geochemistry database analysis, by using the mean of the measured CO_2 values and including 6 wt.% H_2O to saturate the komatiite at greenschist facies conditions. The CO_2 data have an exponential distribution (Supp. Fig. 1), as such the mean is an overestimation of the true distribution of CO_2 (e.g., the median is 0.39 wt% CO_2). However, the database likely has a strong bias away from CO_2-bearing samples. It is difficult to assess the true extent of carbonation of natural komatiites, and the effect this may have on their metamorphism and devolatilisation. Nonetheless, for the komatiite composition with an XCO_2 of 0.1 dolomite is the primary CO_2 phase stable above ~380 °C, and predominately breaks down via reaction with antigorite and talc to tremolite, olivine, H_2O and CO_2, at temperatures of less than 700 °C. Along a thermal gradient of 950 °C/GPa, all CO_2 is released by 590 °C (Fig. 9b). As such, no CO_2 is released above the basalt solidus in typical Archean thermal gradients for this fluid composition. H_2O release above the basalt solidus in this scenario is comparable with the H_2O-only calculation, and is only ~1 wt.% less (4–4.5 wt.%). Therefore, we suggest if altered komatiites with a starting XCO_2 of 0.1 experienced metamorphism, they will still efficiently transport H_2O, but not CO_2, to basaltic suprasolidus conditions. For higher XCO_2 values the effect may be stronger, however a full investigation into the carbonation of komatiites and the effect on fluid release is out of the scope of this study.

In a way, Archean komatiites may have played a similar role as oceanic peridotites do today in transporting water to deep crustal melting conditions, and therefore the formation of new continental crust. In modern settings, peridotites are serpentinised on the ocean floor, and are important carriers of water to sub-arc depths during subduction (Ulmer and Trommsdorff, 1995). Antigorite breakdown at temperatures of ~ 650 °C allows large volumes of water to migrate to the hotter mantle wedge, where partial melting of peridotite forms basalts, which are either the primary melts of arc magmatism and/or can crystallise at the crust-mantle interface to fluid-flux the lower crust (e.g. Rudnick, 1995; Grove

et al., 2012; Collins et al., 2016). Resulting arc magmas are on average andesitic-dacitic in composition, and represent the growth of new continental crust (Taylor and McLennan, 1995; Jagoutz and Kelemen, 2015). This process is controlled by the inverted thermal gradient formed during cold subduction, which allows hydrous minerals to persist to significant depths, and release water into hot and fertile melting conditions. In the Archean, it is difficult to pinpoint the geodynamic scenario(s) responsible for TTG generation and therefore continental crust formation. However, one could envisage that hydrated komatiite-basalt associations (i.e., greenstone belts) were thickened in an oceanic plateau style setting, or underthrust in a hot subduction style setting, to reach temperatures of 670–800 °C for komatiite dehydration and wet basalt melting (e.g. Hartnady et al., 2022). The subsequent magmas have TTG-compositions, and most likely formed the Archean continental crust. We emphasise that the exact geodynamic style of metamorphism is not critical, as the komatiite dehydration reactions are strongly temperature dependent but only weakly pressure dependent (Fig. 5); hence, water release and TTG formation will occur at similar temperatures regardless of the pressure.

6. Conclusions

Petrology and mineral compositional data of representative metamorphosed komatiites and geochemical rock data from a database of approximately 5600 komatiites show that these Archean ultramafic rocks are highly altered, and on average contain 6 wt.% water. Phase equilibria modelling predicts that hydrated komatiites will release their water via breakdown of antigorite, amphibole and chlorite at temperatures ranging across 500 to 800 °C, regardless of the pressure conditions and, therefore, the P–T path experienced by progressively metamorphosed komatiite. Critically, 5 wt.% of this water is released between 670 and 800 °C, which corresponds to temperature conditions allowing for water-present basalt melting. Therefore, we suggest that water released from dehydrating komatiites provided the free water necessary to partially melt large volumes of basalts to form the prominent and expansive TTG suits in the Archean. Even though komatiites make up moderate portions of greenstone belts, they likely played a key role in early crust formation and the Earths' early water cycle.

CRediT authorship contribution statement

Tamblyn R.: Conceptualization, Formal analysis, Investigation, Visualization, Writing – original draft. **Hermann J.:** Conceptualization, Funding acquisition, Investigation, Project administration, Resources, Writing – review & editing. **Hasterok D.:** Formal analysis, Software, Visualization, Writing – review & editing. **Sossi P.:** Resources, Writing – review & editing. **Pettke T.:** Resources, Writing – review & editing. **Chatterjee S.:** Resources, Writing – review & editing.

Declaration of competing interest

The authors declare that they have no known competing financial interests or personal relationships that could have appeared to influence the work reported in this paper.

Data availability

Data will be made available on request.

Acknowledgements

We would like to thank Pierre Lanari, Coralie Vesin and Hugo Dominguez Carranza for their assistance with EPMA analysis. Pierre Lanari is also thoroughly thanked for his help with XMapTools. We thank Joana Vieira Duarte and Balz Kamber for discussions. We thank Rosemary Hickey-Vargas for editorial handling, and Robert Bolhar and an anonymous reviewer are thanked for their thoughtful comments. Jörg Hermann and Renée Tamblyn acknowledge SNF grant 200020-196927 for support of this research, D. Hasterok acknowledges ARC grant DP180104074, P. Sossi thanks the Swiss National Science Foundation (SNSF) via an Ambizione Fellowship (180025) and the Swiss State Secretariat for Education, Research and Innovation (SERI) under contract number MB22.00033, a SERI-funded ERC Starting Grant '2ATMO', and Sukalpa Chatterjee acknowledges SNF grant 196927.

Appendix A. Supplementary material

Supplementary material related to this article can be found online at https://doi.org/10.1016/j.epsl.2022.117982.

References

Arculus, R.J., Ruff, L.J., 1990. Genesis of continental crust: evidence from Island Arcs, granulites, and exospheric processes. In: Granulites and Crustal Evolution. Springer, pp. 7–23.
Arndt, Nicholas, 2003. Komatiites, kimberlites, and boninites. J. Geophys. Res., Solid Earth 108 (B6).
Arndt, Nicholas, Lesher, Michael, Barnes, Steve, 2008. Komatiite. Cambridge University Press.
Bretscher, Annette, Hermann, Joerg, Pettke, Thomas, 2018. The influence of oceanic oxidation on serpentinite dehydration during subduction. Earth Planet. Sci. Lett. 499, 173–184. https://doi.org/10.1016/J.EPSL.2018.07.017.
Brown, Michael, Johnson, Tim, 2018. Secular Change in Metamorphism and the Onset of Global.
Collins, William J., Huang, Hui-Qing, Jiang, Xiaoyan, 2016. Water-fluxed crustal melting produces Cordilleran batholiths. Geology 44 (2), 143–146.
Connolly, J.A.D., 2009. The geodynamic equation of state: what and how. Geochem. Geophys. Geosyst. 10 (10).
Dann, J.C., 2000. The 3.5 Ga Komati Formation, Barberton Greenstone Belt, South Africa, part I: new maps and magmatic architecture. S. Afr. J. Geol. 103 (1), 47–68. https://doi.org/10.2113/103.1.47.
Drummond, M.S., Defant, M.J., 1990. A model for trondhjemite-tonalite-dacite genesis and crustal growth via slab melting: Archean to modern comparisons. J. Geophys. Res., Solid Earth 95 (B13), 21503–21521.
Evans, Katy A., Frost, B. Ronald, 2021. Deserpentinization in subduction zones as a source of oxidation in arcs: a reality check. J. Petrol. 62 (3), 1–32. https://doi.org/10.1093/petrology/egab016.
Foley, Stephen, Tiepolo, Massimo, Vannucci, Riccardo, 2002. Growth of early continental crust controlled by melting of amphibolite in subduction zones. Nature 417 (6891), 837–840.
Furnes, Harald, Dilek, Yildirim, 2022. Archean versus Phanerozoic oceanic crust formation and tectonics: ophiolites through time. Geosyst. Geoenviron. 1 (1), 100004.
Gard, M., Hasterok, D., Hand, M., Cox, G., 2019. Variations in continental heat production from 4 Ga to the present: evidence from geochemical data. Lithos 342, 391–406.
Getsinger, Amanda, Rushmer, Tracy, Jackson, Matt D., Baker, Don, 2009. Generating high Mg-numbers and chemical diversity in Tonalite-Trondhjemite-Granodiorite (TTG) magmas during melting and melt segregation in the continental crust. J. Petrol. 50 (10), 1935–1954. https://doi.org/10.1093/petrology/egp060.
Green, D.H., 1976. Experimental testing of equilibrium partial melting of peridotite under water-saturated, high-pressure conditions. Can. Mineral. 14 (3), 255–268.
Grove, T.L., Till, C.B., Krawczynski, M.J., 2012. The role of H2O in subduction zone magmatism. Annu. Rev. Earth Planet. Sci. 40 (413), 2012.
Hartnady, M.I., Johnson, T.E., Schorn, S., Smithies, R.H., Kirkland, C.L., Richardson, S.H., 2022. Fluid processes in the early Earth and the growth of continents. Earth Planet. Sci. Lett. 594, 117695.
Hasterok, D., Halpin, J.A., Collins, A.S., Hand, M., Kreemer, C., Gard, M.G., Glorie, S., 2022. New maps of global geological provinces and tectonic plates. Earth-Sci. Rev. 231, 104069.
Herzberg, Claude, Asimow, Paul D., Arndt, Nicholas, Niu, Yaoling, Lesher, C.M., Fitton, J.G., Cheadle, M.J., Saunders, A.D., 2007. Temperatures in ambient mantle and plumes: constraints from basalts, picrites, and komatiites. Geochem. Geophys. Geosyst. 8 (2).
Hoffmann, J.E., Nagel, T.J., Muenker, C., Naeraa, T., Rosing, M.T., 2014. Constraining the process of Eoarchean TTG formation in the Itsaq Gneiss Complex, southern West Greenland. Earth Planet. Sci. Lett. 388, 374–386. https://doi.org/10.1016/j.epsl.2013.11.050.

Holland, T.J.B., Powell, R., 2011. An improved and extended internally consistent thermodynamic dataset for phases of petrological interest, involving a new equation of state for solids. J. Metamorph. Geol. 29 (3), 333–383.
Homann, Martin, 2019. Earliest life on Earth: evidence from the Barberton Greenstone Belt, South Africa. Earth-Sci. Rev. 196, 102888.
Jagoutz, O., Kelemen, P.B., 2015. Role of arc processes in the formation of continental crust. Annu. Rev. Earth Planet. Sci. 43, 363–404.
Jenkins, David M., 1981. Experimental phase relations of hydrous peridotites modelled in the system H2O-CaO-MgO-Al2O3,-SiO2. Contrib. Mineral. Petrol. 77 (2), 166–176. https://doi.org/10.1007/BF00636520.
Johnson, Tim E., Brown, Michael, Gardiner, Nicholas J., Kirkland, Christopher L., Smithies, R. Hugh, 2017. Earth's first stable continents did not form by subduction. Nature 543 (7644), 239–242.
Kempf, Elias D., Hermann, Jörg, Connolly, James A.D., 2022. Serpentinite dehydration at low pressures. Swiss J. Geosci. 115 (1). https://doi.org/10.1186/s00015-022-00415-y.
Kendrick, Jillian, Yakymchuk, Chris, 2020. Garnet fractionation, progressive melt loss and bulk composition variations in anatectic metabasites: complications for interpreting the geodynamic significance of TTGs. Geosci. Front. 11 (3), 745–763. https://doi.org/10.1016/J.GSF.2019.12.001.
Lakey, Shayne, Hermann, Jörg, 2022. An experimental study of chlorite stability in varied subduction zone lithologies with implications for fluid production, melting, and diapirism in chlorite-rich mélange rocks. J. Petrol. 63 (4), egac029. https://doi.org/10.1093/petrology/egac029.
Lambert, I.B., Wyllie, P.J., 1972. Melting of gabbro (quartz eclogite) with excess water to 35 kilobars, with geological applications. I. J. Geol. 80 (6), 693–708.
Lanari, Pierre, Vho, Alice, Bovay, Thomas, Airaghi, Laura, Centrella, Stephen, 2019. Quantitative compositional mapping of mineral phases by electron probe microanalyser. Geol. Soc. (Lond.) Spec. Publ. 478 (1), 39–63.
Lanari, Pierre, Vidal, Olivier, De Andrade, Vincent, Dubacq, Benoît, Lewin, Eric, Grosch, Eugene G., Schwartz, Stéphane, 2014. XMapTools: a MATLAB©-based program for electron microprobe X-ray image processing and geothermobarometry. Comput. Geosci. 62, 227–240.
Laurie, A., Stevens, G., 2012. Water-present eclogite melting to produce Earth's early felsic crust. Chem. Geol. 314, 83–95.
Moyen, J., Stevens, Gary, 2006. Experimental Constraints on TTG Petrogenesis: Implications for Archean Geodynamics. Geophysical Monograph, vol. 164. American Geophysical Union, p. 149.
Moyen, Jean François, Martin, Hervé, 2012. Forty years of TTG research. Lithos 148, 312–336. https://doi.org/10.1016/J.LITHOS.2012.06.010.
Nesbitt, R.W., Sun, S.S., 1976. Geochemistry of Archaean spinifex-textured peridotites and magnesian and low-magnesian tholeiites. Earth Planet. Sci. Lett. 31 (3), 433–453.
Nesbitt, Robert W., Sun, Shen-Su, Purvis, A.C., 1979. Komatiites: geochemistry and genesis. Can. Mineral. 17, 165–186.
Parman, Stephen W., Grove, Timothy L., Dann, Jesse C., De Wit, Maarten J., 2004. A subduction origin for komatiites and cratonic lithospheric mantle. S. Afr. J. Geol. 107 (1–2), 107–118.
Polat, A., 2012. Growth of Archean continental crust in oceanic island arcs. Geology 40 (4), 383. https://doi.org/10.1130/focus042012.1.
Pourteau, Amaury, Doucet, Luc S., Blereau, Eleanore R., Volante, Silvia, Johnson, Tim E., Collins, William J., Li, Zheng-Xiang, Champion, David C., 2020. TTG generation by fluid-fluxed crustal melting: direct evidence from the Proterozoic Georgetown Inlier, NE Australia. Earth Planet. Sci. Lett. 550, 116548.
Qian, Qing, Hermann, Jörg, 2013. Partial melting of lower crust at 10–15 Kbar: constraints on adakite and TTG formation. Contrib. Mineral. Petrol. 165 (6), 1195–1224. https://doi.org/10.1007/s00410-013-0854-9.
Rapp, Robert P., Watson, E. Bruce, 1995. Dehydration melting of metabasalt at 8–32 Kbar: implications for continental growth and crust-mantle recycling. J. Petrol. 36 (4), 891–931.
Rapp, Robert Paul, Watson, E. Bruce, Miller, Calvin F., 1991. Partial melting of amphibolite/eclogite and the origin of Archean trondhjemites and tonalites. Precambrian Res. 51 (1–4), 1–25. https://doi.org/10.1016/0301-9268(91)90092-O.
Rudnick, Roberta L., 1995. Making continental crust. Nature 378 (6557), 571–578.
Sossi, Paolo A., Eggins, Stephen M., Nesbitt, Robert W., Nebel, Oliver, Hergt, Janet M., Campbell, Ian H., O'Neill, Hugh St C., Van Kranendonk, Martin, Rhodri Davies, D., 2016. Petrogenesis and geochemistry of Archean komatiites. J. Petrol. 57 (1), 147–184. https://doi.org/10.1093/petrology/egw004.
Spandler, Carl, Hermann, Jörg, Faure, Kevin, Mavrogenes, John A., Arculus, Richard J., 2008. The importance of talc and chlorite 'hybrid' rocks for volatile recycling through subduction zones; evidence from the high-pressure subduction mélange of New Caledonia. Contrib. Mineral. Petrol. 155 (2), 181–198.
Staudigel, H., Schreyer, W., 1977. The upper thermal stability of Clinochlore, Mg5Al[AlSi3O10](OH)8, at 10-35 Kb PH2O. Contrib. Mineral. Petrol. 61 (2), 187–198.
Taylor, Stuart Ross, McLennan, Scott M., 1995. The geochemical evolution of the continental crust. Rev. Geophys. 33 (2), 241–265.
Ulmer, P., Trommsdorff, V., 1995. Serpentine stability to mantle depths and subduction-related magmatism. Science 268 (5212), 858–861.
Vieira Duarte, J.F., Piccoli, F., Pettke, T., Hermann, J., 2021. Textural and geochemical evidence for magnetite production upon antigorite breakdown during subduction. J. Petrol. 62 (10), egab053.
Wilson, Allan H., 2019. The late-paleoarchean ultra-depleted commondale komatiites: Earth's hottest lavas and consequences for eruption. J. Petrol. 60 (8), 1575–1620.
Wilson, Allan, Bolhar, Robert, 2022. Olivine in komatiite records origin and travel from the deep upper mantle. Geology 50 (3), 351–355.
Wyllie, Peter J., Wolf, Michael B., 1993. Amphibolite Dehydration-Melting: Sorting Out the Solidus. Geological Society Special Publication, vol. 76, pp. 405–416.
Xiong, Xiaolin, Keppler, Hans, Audétat, Andreas, Gudfinnsson, Gudmundur, Sun, Weidong, Song, Maoshuang, Xiao, Wansheng, Yuan, Li, 2009. Experimental constraints on rutile saturation during partial melting of metabasalt at the amphibolite to eclogite transition, with applications to TTG genesis. Am. Mineral. 94 (8–9), 1175–1186. https://doi.org/10.2138/am.2009.3158.
Zhang, Chao, Holtz, Francois, Koepke, Jürgen, Eric, Paul, Ma, Changqian, Bédard, Jean H., 2013. Constraints from experimental melting of amphibolite on the depth of formation of garnet-rich restites, and implications for models of early Archean crustal growth. Precambrian Res. 231, 206–217. https://doi.org/10.1016/j.precamres.2013.03.004.